ChemPubSoc Europe

DOI: 10.1002/chem.201803807

CHEMISTRY A European Journal Full Paper

Check for updates

Rare-Earth or f-Element Chemistry

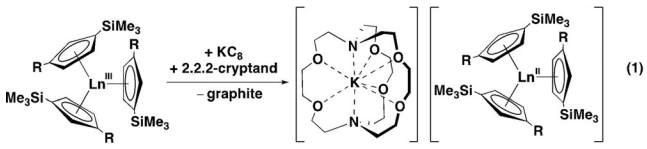
Rare-Earth Metal(II) Aryloxides: Structure, Synthesis, and EPR Spectroscopy of [K(2.2.2-cryptand)][Sc($OC_6H_2tBu_2$-2,6-Me-4)$_3$]

Samuel A. Moehring,[a] María J. Beltrán-Leiva,[b] Dayán Páez-Hernández,[b] Ramiro Arratia-Pérez,[b] Joseph W. Ziller,[a] and William J. Evans*[a]

Abstract: The suitability of aryloxide ligands for stabilizing +2 oxidation states of Sc and Y has been examined and EPR evidence indicating the first O-donor complexes of Sc^{II} and Y^{II} has been obtained, as well as an X-ray crystal structure of a Sc^{II} aryloxide complex. The trivalent rare-earth metal aryloxide precursors, Ln(OAr′)$_3$, **1-Ln** (Ln = Sc, Y, Gd, Dy, Ho, Er; OAr′ = $OC_6H_2tBu_2$-2,6-Me-4), were synthesized from the corresponding rare-earth metal trichlorides and LiOAr′·OEt_2. Reduction of THF solutions of **1-Ln** with potassium graphite in the presence of 2.2.2-cryptand (crypt) yielded dark-colored solutions, **2-Ln**, whose EPR spectra at 77 K are characteristic of the Ln^{II} ions: a two-line spectrum ($g_{\parallel}$ = 1.99, $g_{\square}$ = 1.97, A_{ave} = 154 G) for **2-Y** and an eight-line spectrum (g_{ave} = 2.01 and A_{ave} = 291 G) for **2-Sc**. Solutions of **2-Y** decompose within one minute at room temperature, wheras **2-Sc** persists up to 40 min at room temperature. **2-Sc** was identified by X-ray crystallography as [K(crypt)][Sc(OAr′)$_3$], which has a trigonal-planar arrangement of oxygen-donor atoms around Sc^{II}. Analogous reductions of **1-Ln** for Ln = Gd, Dy, Ho, and Er also gave dark solutions of limited stability. Theoretical analysis using time-dependent density functional theory (TD-DFT) along with complete active space self-consistent field (CASSCF) methods, and structural analysis with the Guzei ligand solid angle *G*-parameter method are presented.

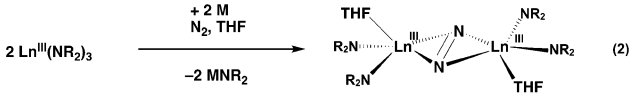
Introduction

The reductive chemistry of the rare-earth elements has been investigated along two lines in recent years. LnA_3/M reduction reactions (Ln = Sc, Y, lanthanides; A = anionic ligand; M = alkali metal) have been conducted under argon to isolate complexes of new Ln^{II} ions,[1–9] for example, with A = $C_5H_4SiMe_3$ and $C_5H_3(SiMe_3)_2$ in [Eq. (1)], and under dinitrogen to make reduced dinitrogen complexes of $(N_2)^{2-}$, [Eq. (2)],[10] and the first examples of $(N_2)^{3-}$.[11,12]



(1)

R = H, Ln = Y, La, Ce, Pr, Nd, Gd, Tb, Dy, Ho, Er, and Lu
R = $SiMe_3$, Ln = La, Ce, Pr, and Nd



Ln = Y, Nd, Gd, Tb, Dy, Ho, Er, Tm, Lu
M = Na, K, or KC_8

As these studies progressed, a pattern developed. Reactions with A = silylcyclopentadienyl ligands[13] such as $C_5H_4SiMe_3$ and $C_5H_3(SiMe_3)_2$ under Ar gave crystallographically-characterizable Ln^{II} complexes, [Eq. (1)].[1,2,4–6] Reactions with A = NR_2 (R = $SiMe_3$) on the other hand, did not give isolable Ln^{II} complexes under Ar, but readily provided $(N_2)^{2-}$ and $(N_2)^{3-}$ complexes when performed under N_2, [Eq. (2)].[10–12] A deviation from this pattern, however, was recently reported with the isolation of [K(2.2.2-cryptand)][Ln(NR_2)$_3$] complexes for Ln = Sc[14] and the lanthanides,[15] but not yttrium. This dichotomy in reactivity spurred on further investigations into ligand effects on reactions accessible through the LnA_3/M method.

Reactions using the aryloxide ligand OAr (OAr = $OC_6H_3tBu_2$-2,6) were important in the initial discovery of complexes containing the $(N_2)^{3-}$ radical trianion.[11,12] The first example of a $(N_2)^{3-}$ complex was synthesized from a reaction of DyI_2 with KOAr under a N_2 atmosphere and later examples were obtained using the LnA_3/M reactions with Dy(OAr)$_3$, [Eq. (3)].[11]

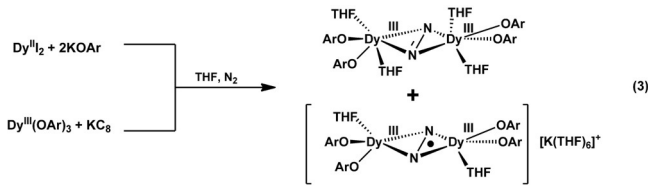
However, once the success of the A = NR_2 ligand in the LnA_3/M reactions under dinitrogen was established, reductive chemistry with aryloxide ligands was not developed further. This study addresses that deficiency. Reductions of tris(aryloxide) rare-earth metal complexes are also of interest in light of recent results with the tris(aryloxide)arene ligand,

[a] S. A. Moehring, Dr. J. W. Ziller, Prof. Dr. W. J. Evans
Department of Chemistry, University of California, Irvine
1102 Natural Sciences II, Irvine, CA 92697-2025 (USA)
E-mail: wevans@uci.edu

[b] M. J. Beltrán-Leiva, Dr. Prof. D. Páez-Hernández, Dr. Prof. R. Arratia-Pérez
Relativistic Molecular Physics (ReMoPh) Group
Ph.D. Program in Molecular Physical Chemistry
Universidad Andrés Bello
Av. República 275, Santiago 8370146 (Chile)

Supporting information and the ORCID identification number(s) for the author(s) of this article can be found under:
https://doi.org/10.1002/chem.201803807.

© 2018 Wiley-VCH Verlag GmbH & Co. KGaA, Weinheim



(3)

((^{Ad,Me}ArO)$_3$mes)$^{3-}$, which has proven to be a suitable ligand for isolating Ln^{II} complexes as well as +2 ions of the actinides.[16–18]

In this study, rare-earth metals whose +2 oxidation states would be easily identifiable by EPR spectroscopy, specifically Y and Sc, were investigated to probe the suitability of the tris(aryloxide) ligand set for isolating Ln^{II} rare-earth metal complexes. This approach has the extra advantage that these metals can be characterized by NMR spectroscopy in their +3 oxidation states owing to their diamagnetism. Additionally, to exclude any reactivity possible with the 4-position of OAr ligands,[19] the 4-methyl-substituted analog of OAr, namely OC$_6$H$_2$*t*Bu$_2$-2,6-Me-4 (OAr′), was explored.

Results and Discussion

Yttrium: Y(OAr′)$_3$, **1-Y**, the precursor for the reduction described below, was prepared from YCl$_3$ and LiOAr′·OEt$_2$ following literature procedures.[20,21] The complex was crystallographically characterized and found to crystallize in $P\bar{1}$ with five independent molecules in the unit cell, Figure 1 and Figure 2. The five molecules have similar Y–O distances, with a range of 2.032(2)–2.053(2) Å and an average of 2.045(7) Å, but they differ significantly in the distances of the Y atom from the plane of the three donor O atoms. Two extreme examples are shown in Figure 2. The yttrium displacements from the O$_3$ plane are 0.009, 0.014, 0.019, 0.449, and 0.479 Å in the five molecules. The angles of the phenyl rings of the ligands with the plane of the three oxygen atoms are quite variable and

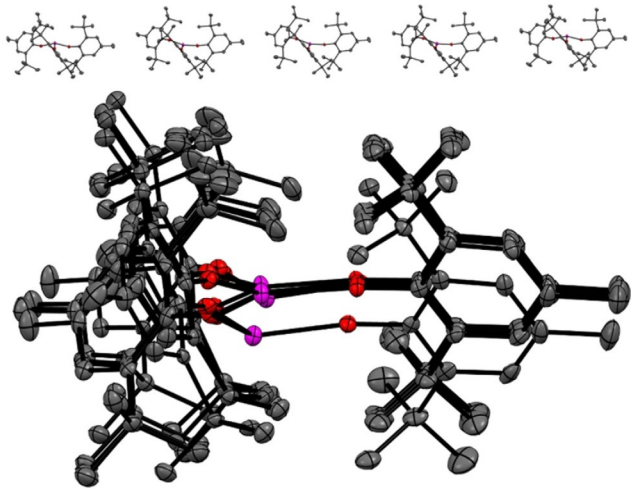


Figure 1. Thermal ellipsoid plots of **1-Y** from the side (top) and along the axis of the 5 Y atoms (bottom). Hydrogen atoms have been removed for clarity. Thermal ellipsoids are drawn at the 50% probability level.

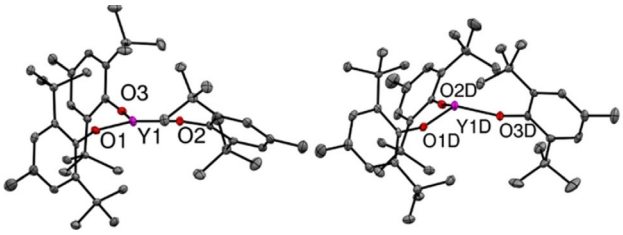


Figure 2. Representative thermal ellipsoid plots of two of the five molecules in the unit cell of **1-Y**, one planar (left) and one pyramidalized (right). Hydrogen atoms have been removed for clarity. Thermal ellipsoids are drawn at the 50% probability level.

range from 39.71–77.93°. The six quaternary carbons of the *tert*-butyl groups of the three OAr′ ligands form a distorted octahedron around the yttrium.

Y(OAr′)$_3$, **1-Y**, reacts at −30 °C with potassium graphite (KC$_8$) in THF in the presence of 2.2.2-cryptand (crypt) to form a dark blue solution, **2-Y**, analogous to that found in the synthesis of the crystallographically-characterizable Y^{II} complex, [K(crypt)][Cp′$_3$Y] (Cp′ = C$_5$H$_4$SiMe$_3$) in [Eq. (1)] under similar conditions.[2] Complex **2-Y** decomposes in ca. one minute at room temperature. Even at −30 °C, **2-Y** fades to a clear, colorless solution in minutes and growing crystals at −78 °C has not been successful.

To obtain EPR data on **2-Y**, a sample was prepared at −30 °C, removed from the glovebox, and frozen in liquid nitrogen within a 45 second time span. The product displays a two-line axial EPR spectrum at 77 K with $g_{\parallel} = 1.99$, $g_{\square} = 1.97$, and $A_{ave} = 154$ G, Figure 3, consistent with an unpaired electron interacting with a 100% abundant $I = 1/2$ ^{89}Y nucleus.[4] The UV/Visible spectrum of **2-Y** has a single broad absorbance at 704 nm with $\varepsilon = 6500\ M^{-1}\ cm^{-1}$, Figure 4. This is more intense than that measured for the crystallographically-characterized [K(crypt)][Cp′$_3$Y], $\varepsilon = 4500\ M^{-1}\ cm^{-1}$.[2] The EPR and optical spectra are consistent with the presence of 4d^1 Y^{II} complex in solution.

The importance of substituting the 4-position of the aryloxide was probed by examining the reduction of Y(OAr)$_3$, **3-Y**,[22] with KC$_8$ in the presence of crypt. Complex **3-Y** reacted similarly to **1-Y** forming a dark-colored solution, **4-Y**, that also had limited thermal stability, similar to that of **2-Y**. The EPR spec-

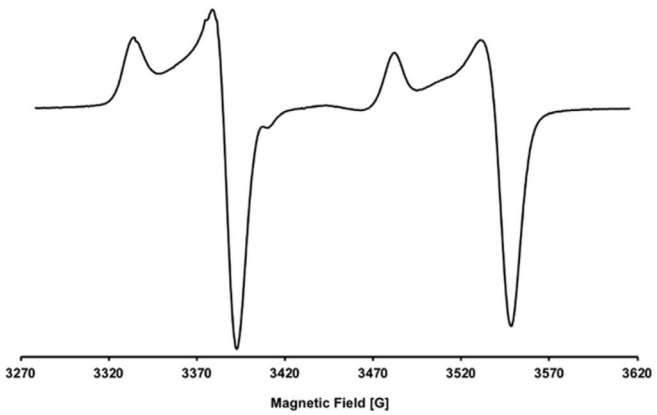


Figure 3. 77 K X-band EPR spectrum of **2-Y**.

© 2018 Wiley-VCH Verlag GmbH & Co. KGaA, Weinheim

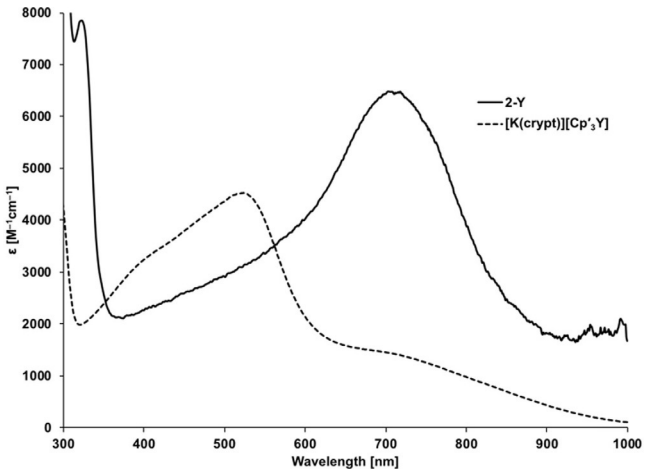


Figure 4. UV/Visible spectrum of **2-Y** in THF at −78 °C and [K(crypt)][Cp'_3Y] in THF at room temperature.

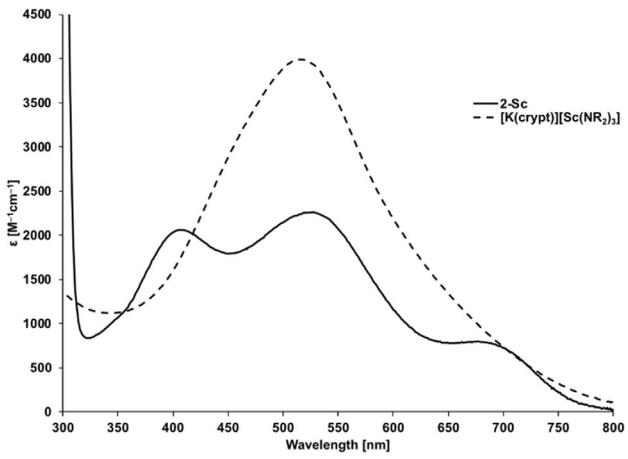


Figure 6. UV/Visible spectrum of **2-Sc** in THF at −78 °C and [K(crypt)][$Sc(NR_2)_3$] in THF at room temperature. R = $SiMe_3$.

trum of **4-Y** at 77 K was nearly identical to that of **2-Y** with $g_{\parallel} = 1.99$, $g_{\square} = 1.97$, and $A_{ave} = 156$ G (Figure S5, Supporting Information). Evidently, the substituent on the 4-position of the aryloxide ligand does not appreciably perturb the KC_8 reactivity of the complexes or the stability of the product.

Scandium: $Sc(OAr')_3$, **1-Sc**, was prepared like **1-Y**, from $ScCl_3$ and $LiOAr'{\cdot}OEt_2$ following literature methods.[20,21,23] $Sc(OAr')_3$, **1-Sc**, also reacts at −30 °C with KC_8 in THF in the presence of crypt to form a dark maroon solution, **2-Sc**. In contrast to the thermal instability of **2-Y** and **4-Y**, the deep maroon color of **2-Sc** persists after 40 minutes at room temperature, and for days at −30 °C in the glovebox. EPR analysis of **2-Sc** at 77 K showed an eight-line pattern with $g_{ave} = 2.01$ and $A_{ave} = 291$ G, Figure 5, which would be expected for a Sc^{II} species having an unpaired electron interacting with a 100% abundant $I = 7/2$ ^{45}Sc nucleus[14,24,25] The UV/Visible absorption spectrum of **2-Sc** has several strong absorptions from 327–677 nm, Figure 6, with molar extinction coefficients from 790–2300 $M^{-1}\,cm^{-1}$. The spectrum of [K(crypt)][$Sc(NR_2)_3$] (R = $SiMe_3$) is shown for comparison.[14] These spectra are consistent with the presence of a $3d^1$ Sc^{II} complex.

Crystals of **2-Sc** could be isolated by crystallization from a THF-pentane mixture and X-ray crystallography revealed the presence of [K(crypt)][$Sc(OAr')_3$], Figure 7, a Sc^{II} complex as expected based on its EPR spectrum. The $[K(crypt)]^+$ cation is well-separated from the $[Sc(OAr')_3]^-$ anion and 3.5 molecules of THF per unit cell are found in the lattice. The three oxygen donor atoms of the OAr′ ligands form a trigonal planar array around Sc with O-Sc-O angles of 117.30(6), 121.89(7), and 120.75(7)°. The Sc center is within 0.03 Å of the plane of these three oxygen atoms. The aryl rings of the OAr′ ligands are canted with respect to the O_3 plane by angles of 61.11, 63.16, and 63.67° such that there are three *tert*-butyl groups above the plane and three below. The six quaternary carbons of the *tert*-butyl groups define a distorted octahedron. The 1.960(2)–1.964(2) Å Sc–O distances in **2-Sc** are substantially larger than the 1.853–1.889 Å distances in the precursor, $Sc(OAr')_3$, **1-Sc**.[23]

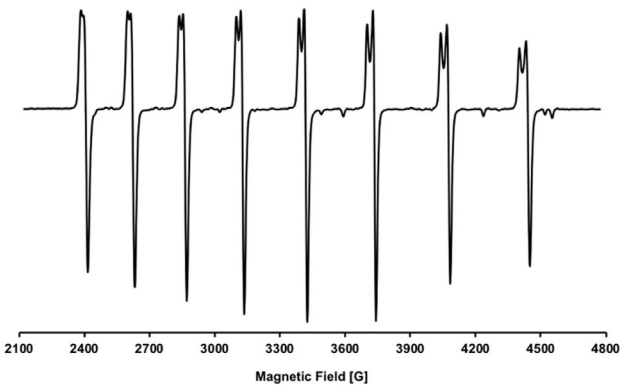


Figure 5. 77 K X-band EPR spectrum of **2-Sc**.

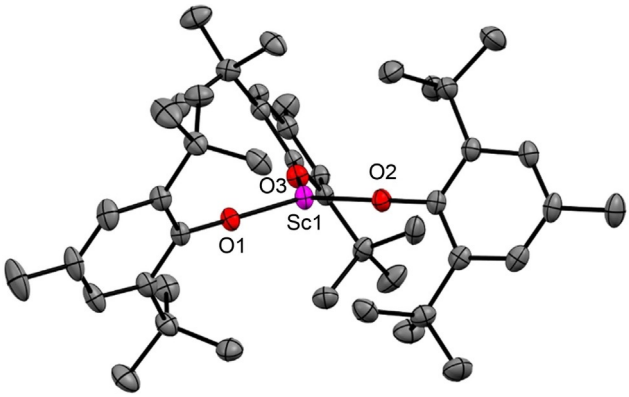


Figure 7. Thermal ellipsoid plot of **2-Sc**. Hydrogen atoms, the $[K(crypt)]^+$ counter-cation, and 3.5 molecules of lattice THF have been removed for clarity. Thermal ellipsoids are drawn at the 50% level.

Lanthanides: The lanthanide complexes $Ln(OAr')_3$ (Ln = Gd, Dy, Ho, Er) were also reacted with KC_8 at −30 °C in THF in the presence of crypt to form deep purple solutions, **2-Ln**. These solutions had intermediate stability between **2-Sc** and **2-Y**, maintaining their deep color for about 1 day at −30 °C. Their UV/Visible spectra are similar to each other, and have strong,

© 2018 Wiley-VCH Verlag GmbH & Co. KGaA, Weinheim

broad absorptions near 450 and 600 nm, Figure 8. The UV/Visible spectra of [K(crypt)][Cp′$_3$Ln] are presented alongside for comparison.[2]

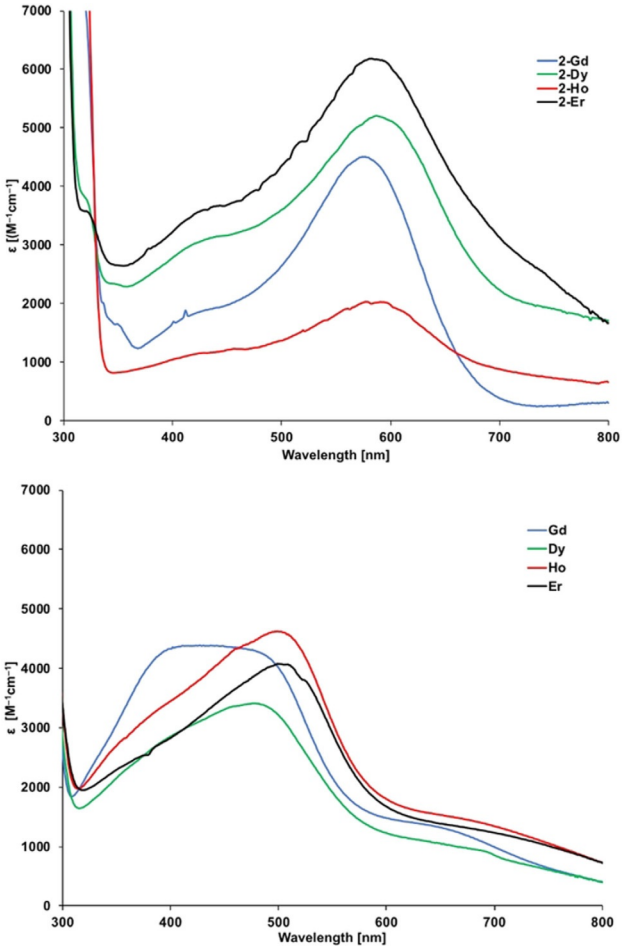


Figure 8. UV/Visible spectra of **2-Ln** at −78 °C in THF (top) and [K(crypt)][Cp′$_3$Ln] in THF at room temperature (bottom).

Theoretical Analysis: Geometry optimizations were carried out to model a possible structure for **2-Y** in lieu of an X-ray diffraction structure. The optimized structure of "[Y(OAr′)$_3$]$^-$" is shown in Figure 9 and the oxygen atoms form a trigonal plane around the metal. Furthermore, as expected due to the homoleptic nature of the complex, all the Y–O distances are ≈2.135 Å and the O-Y-O angles are ≈120°. In the time-dependent DFT (TD-DFT) simulated UV/Visible spectrum, the experimental λ_{max} at 704 nm was reproduced properly at ≈675 nm (Figure S3, Supporting Information). This band was characterized as a MLCT band, because an almost pure d→π transition was observed from the molecular orbital plots (Figure S4, Supporting Information). The SOMO of the complex has a predominant d_{z^2} character and shows antibonding interactions with the orbitals from the closest C–H bonds from methyl groups. These results are consistent with those reported for (Cp′$_3$Y)$^-$ regarding the assignment of the main transition bands, which have an important d→π (MLCT) character.[4,5] However, in this

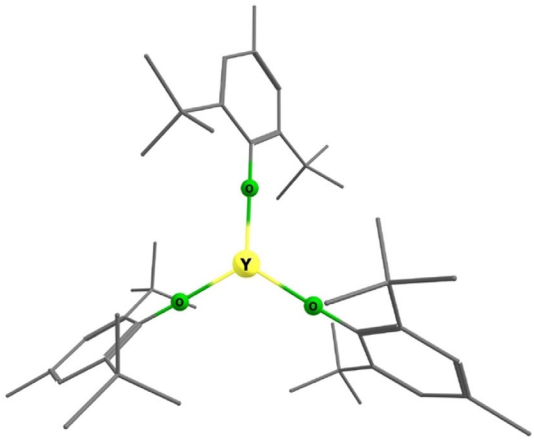


Figure 9. DFT-optimized structure of [Y(OAr′)$_3$]$^-$.

tris(aryloxide) environment, a bathochromic shift is predicted by the calculations and observed experimentally.

The same calculations were performed on **2-Sc**. As with **2-Y**, all three Sc–O bonds have the same length, 1.98 Å, which matches the experimental bond length range of 1.960(2)–1.964(2) Å. All the O-Sc-O angles measure ca. 120°, close to the observed range of 117.30(6)–121.89(7)°. The difference between the bond lengths relative to the yttrium system is consistent with the difference in the ionic radii of these elements (ca. 0.15 Å).[26] The calculated absorption spectrum is in good agreement with the experimental one (Figure S5, Supporting Information). The three main bands in Figure 6 were correctly predicted with an error of around 35 nm (Figure S6 and Table S7), which is the normal range for DFT calculations. The two most intense bands that appear at 365 and 497 nm, respectively, have an almost pure d→π character and therefore could be classified as MLCT bands, whereas the weak transition at 661 nm is predominantly d→d*. This assignment is consistent with that obtained for [Sc(NR$_2$)$_3$]$^-$ with D_3 symmetry.[14] The bands located in the UV region are due to absorptions produced by the aryloxide ligands.

To get a deeper insight into the analysis of the lanthanide complexes, possible structures for **2-Ln** were modeled based on the previous systems. As in case of yttrium and scandium complexes, the structural parameters of the modeled **2-Ln** complexes (Table S5) show features characteristic of homoleptic systems. The SOMOs of **2-Gd**, **2-Er** and **2-Ho** have d_{z^2} character, as found earlier for the [Cp′$_3$Ln]$^-$ complexes[2,5] which predict a $4f^n5d^1$ configuration for these kinds of compounds with trigonal symmetry. The simulated absorption spectra for **2-Gd**, **2-Er** and **2-Ho** properly reproduce the experimental results and describe with only minimal error the broad band located between 450 and 600 nm. However, in **2-Dy** the DFT calculation shows a SOMO with a marked f character, which means that in this case the dominant configuration is $4f^{10}$. On the other hand, the simulated absorption spectrum exhibits an unexpected bathochromic shift of ca. 100 nm, which could be attributed to an incorrect prediction of the ground state nature in **2-Dy** and the inherent delocalization error at the DFT level. Previous studies[27–29] have demonstrated that an excess

© 2018 Wiley-VCH Verlag GmbH & Co. KGaA, Weinheim

in the 4f populations arises from ligand donation, along with donation into the 5d shell. Thus, DFT calculations for systems with an incomplete 4f shell produce several degrees of excess in the 4f populations, which can produce an erroneous interpretation of the spectroscopic properties. For this reason, more accurate calculations are necessary to properly understand the nature of the ground state of these compounds and correctly assign the absorption spectra.

To corroborate and clarify the previous analysis, multiconfigurational complete active space self-consistent field along with second order perturbation theory (CASSCF/PT2) calculations were performed on **2-Ln** in order to elucidate the nature of their ground states. In agreement with the DFT results, **2-Gd**, **2-Er** and **2-Ho** have a 100% $4f^n5d^1$ configuration as expected from the experimental UV/Vis spectra and previous works, where these lanthanides were classified as $4f^n5d^1$ ions.[3] In case of **2-Dy**, the situation is more complicated, because according to the DFT analysis, the ground state configuration should be $4f^{10}$, but this disagrees with the similarity observed between its spectra and those of **2-Gd**, **2-Er** and **2-Ho**. Furthermore, Dy has been classified as configurational crossover ion which increases the doubt about the DFT results.[3] According to the CASSCF/PT2 study, **2-Dy** has a 100% $4f^95d^1$ configuration, which supports the experimental observation. This is a more reliable result, considering the high performance of the CASSCF/PT2 methodology in the treatment of heavy elements and the deficiencies of the DFT. In all the **2-Ln** systems, the ground multiplet is completely isolated from the excited ones, which is common in lanthanide compounds. These results agree with the experimental UV/Visible spectra for Ln^{II} systems in the $(Cp')_3$ environment, where they were classified as $4f^n5d^1$ ions.[3]

Structural Analysis by the Method of Guzei: To explore a steric rationale for the large difference in thermal stability between **2-Y** and **2-Sc**, as well as the difference in thermal stability between **2-Y** and other Y^{II} complexes,[2,4,30] the Solid-G analysis method of Guzei[34] was used to compare the degree of steric saturation afforded by cyclopentadienyl, aryloxide, and amide ligands, Table 1. This method provides an estimation of the percentage of the coordination sphere of the metal that is protected by the ligands by evaluating the solid angle generated by the ligands. *G*-parameters are calculated for each compound from the crystal structure data on that compound. A *G*-parameter of 100% indicates that the ligands completely shield the metal from exogenous substrates, whereas a *G*-parameter of 50% means that the ligands cover only half the coordination sphere of the metal.

The *G*-parameters calculated for the complexes that have been crystallographically characterized in Table 1 range from 81 to 92%. In comparison, the value calculated from the structure computed by DFT for the putative "$[Y(OAr')_3]^-$", which has not been isolated, is only 77%. As a calibration on these numbers, the *G*-parameter for $Cp_3Y(THF)$, which can be readily isolated and crystallized, is 83%. The *G*-parameter for the imaginary molecular "Cp_3Y" is 71%. When unsolvated "Cp_3Y" crystallizes, it is isolated as a coordination polymer, $[(\eta^5\text{-Cp})_2Y(\mu\text{-}\eta^5\text{:}\eta^1\text{-Cp})]_n$.[31]

Discussion

EPR Spectra: The two-line signals present in the EPR spectra of **2-Y** (Figure 1) and **4-Y** (Figure S1 in Supporting Information) are consistent with the presence of a $4d^1$ Y^{II} complex in solution. As shown in Table 2, the *g*-values are similar to other solutions obtained by reducing Y^{III} complexes with KC_8 in THF. However, the 154 and 158 G hyperfine coupling constants are substantially higher than those of the only other crystallographically-characterized Y^{II} complexes, $[K(18\text{-crown-6})][Cp'_3Y]$, 36.6 G, and $[K(crypt)][Cp''_2Y(C_5H_5)]$, 34.6 G ($Cp' = C_5H_4SiMe_3$, $Cp'' = C_5H_3(SiMe_3)_2$-1,3).

The large yttrium hyperfine coupling constants are consistent with a previous correlation that the stability of solutions obtained by reducing Y^{III} decreases as the hyperfine coupling constant increases.[30] The rationale was that the larger the *A*

Table 1. *G*-parameters and bond metrics for rare-earth metal complexes.

Complex	Ln-donor atom or Ln-centroid range [Å]	Average Ln-centroid or Ln-donor atom [Å]	*G* [%]	Ref.
$Sc(OAr')_3$	1.8530–1.8886	1.8685	90	[23]
$Y(OAr')_3$	2.042(2)-2.053(2)	2.045(7)	81-82[h]	this work
$[Sc(OAr')_3]^-$	1.961(2)-1.964(2)	1.962(3)	83	this work
"$[Y(OAr')_3]^-$"[a]	2.1351–2.1353	2.1352	77	this work
$Sc(NR_2)_3$[b]	2.048(2)-2.057(2)	2.052(3)	87	[14]
$[Sc(NR_2)_3]^-$	2.116(1)-2.137(2)	2.129(2)	84	[14]
Cp'_3Y[c]	2.403–2.409	2.405	86	[4]
$[Cp'_3Y]^-$	2.428–2.443	2.436	86	[4]
$Cp^{Me}_3Y(THF)$[d]	2.443–2.459	2.451	87	[30]
"Cp_3Y"[e,f]	2.373–2.503	2.431	71–72[h]	[31]
$Cp_3Y(THF)$	2.438–2.455	2.449	83	[32]
$[Cp''_2YCp]^-$[g]	Cp: 2.426–2.436 Cp'': 2.421–2.468	Cp: 2.432 Cp'': 2.440	90–91[h]	[30]
Cp''_3Y	2.424–2.428	2.425	92	[33]

Crystal structure data of the rare-earth containing molecules and ions were input into the Solid-G program excluding any lattice solvent or counterions for all the entries except [a] "$[Y(OAr')_3]^-$", which is based on an optimized geometry from DFT calculations, and [g] "Cp_3Y" whose range comes from calculation of the two "Cp_3Y" units in the unit cell of polymeric $[(\eta^5\text{-Cp})_2Y(\mu\text{-}\eta^5\text{:}\eta^1\text{-Cp})]_n$. [b] R = $SiMe_3$. [c] $Cp' = C_5H_4SiMe_3$. [d] $Cp^{Me} = C_5H_4Me$. [e] $Cp = C_5H_5$. [g] $Cp'' = C_5H_3(SiMe_3)_2$-1,3. [h] Unit cell contains multiple molecules.

© 2018 Wiley-VCH Verlag GmbH & Co. KGaA, Weinheim

Table 2. Comparison of EPR parameters of reduction products of YX_3 complexes (X = anion)

Compound Reduced	g_{ave}	A [G]	Ref
Cp''_2YCp[a,b]	1.99	34.6	[30]
Cp''_3Y	1.99	36.1	[30]
Cp''_2YCp^{Me}[c]	1.99	36.4	[30]
Cp'_3Y[d]	1.99	36.6	[4]
$Cp_3Y(THF)$	1.99	42.8	[30]
$Cp^{Me}{}_3Y(THF)$	1.99	46.9	[30]
$Y(NR_2)_3$ [e]	1.98	110	[30]
$Y(OAr')_3$	1.98	154	this work
$Y(OAr)_3$	1.98	156	this work

[a] $Cp'' = C_5H_3(SiMe_3)_2$-1,3. [b] $Cp = C_5H_5$. [c] $Cp^{Me} = C_5H_4Me$. [d] $Cp' = C_5H_4SiMe_3$. [e] $R = SiMe_3$.

values, the more electron density that is localized on the metal center and the more reactive it becomes. The hyperfine coupling constants of **2-Y** and **4-Y** are even larger than the 110 G value for the $Y(NR_2)_3$ reduction product,[12] which suggests that the OAr′ and OAr ligands put the most electron density on the metal compared to all the ligands surveyed to date.

It should be noted that crystals of "$(Cp''_3Y)^-$" were also not isolated, although its A value of 36.1 G is between of the values of the crystallographically-characterized [K(18-crown-6)][Cp'_3Y][4] and [K(crypt)][Cp''_2YCp].[30] This indicates that factors other than those affecting A values must be operative in affecting the stability of the Ln^{II} complexes. In this "$(Cp''_3Y)^-$" case, it likely that steric factors are involved as described below.

In the case of scandium, both the EPR spectrum and the X-ray crystal structure of **2-Sc** are consistent with a Sc^{II} complex. The eight-line EPR-spectrum of **2-Sc** is similar to that of crystallographically-characterized [K(crypt)][$Sc(NR_2)_3$],[14] and the 291 G hyperfine value for **2-Sc** is higher than the 225 G value for [K(crypt)][$Sc(NR_2)_3$]. This is consistent with the trend shown in Table 2 for the yttrium aryloxides versus yttrium amide. The A value for **2-Sc** is also larger than those found for the Sc^{II} complexes $Sc(\eta\text{-}t\text{Bu}_3C_6H_3)(\eta^6\eta^1\text{-}t\text{Bu}_2[CMe_2CH_2]C_6H_3)H$ ($A = 13.45$ G)[25] and $Sc(\eta^5\text{-}P_2C_3t\text{Bu}_3)_2$ ($A_{\square} = 29.9$ G, $A_{\parallel} = 52.9$).[24]

Sc Structure: The average Sc–O bond distances in [K(crypt)][$Sc(OAr')_3$], **2-Sc**, are 0.09 Å larger than those in the Sc^{III} precursor, $Sc(OAr')_3$, **1-Sc**.[23] Comparison of the $Cp'_3Ln^{III}/[Cp'_3Ln^{II}]^-$ series of Eq. (1) showed differences in Ln-ligand distances of only 0.03 Å for Ln^{II} ions that had $4f^n5d^1$ electron configurations and 0.1–0.2 Å for Ln^{II} that had $4f^{n+1}$ configurations (i.e., the traditional Ln^{II} ions of Eu, Yb, Sm, and Tm).[2,3] The increase in Sc–O distance from Sc^{III} to Sc^{II} with these aryloxides is in between these two ranges, even though scandium has no f orbitals. The 0.08 Å difference in Sc–N bond distances of $Sc^{III}(NR_2)_3$ and [K(crypt)][$Sc^{II}(NR_2)_3$] ($R = SiMe_3$) is similar[14] to that of the aryloxides. Hence, care must be taken in assigning electron configurations for new Ln^{II} ions solely on the basis of the difference in bond distances for Ln^{III} versus Ln^{II}.

UV/Visible Spectra: The UV/Visible spectrum of **2-Y** (Figure 4) has a single strong feature in the visible region, with an extinction coefficient of 6500 M^{-1} cm^{-1}, greater than those of **2-Sc** (2300 M^{-1} cm^{-1}) and the $[Cp'_3Ln]^-$ complexes in eq 1 (ca. 5000 M^{-1} cm^{-1}).[2] In contrast, **2-Sc** (Figure 6) shows several strong absorptions in the visible region which differs from that of [K(crypt)][$Sc(NR_2)_3$] and the $[Cp'_3Ln]^-$ (Ln = Y, Pr, Gd, Tb, Ho, Er, and Lu) complexes which have only a single feature in the same region. The solutions of **2-Ln** have spectra that have a single strong feature plus a shoulder, in contrast to the single feature of the $[Cp'_3Ln]^-$ in Eq. (1).[2,3,14]

The simulated spectra properly reproduce the experimental data for most of the studied systems, where the main absorptions were characterized as MLCT bands which has been previously noted for these ions in tris(cyclopentadienyl) environments.[2,5] As explained above, in **2-Dy** the spectrum was not correctly assigned at the DFT level because of problems with the prediction of its ground state nature. However, this was corrected when the electron correlation was included through CASSCF/PT2 calculations.

Guzei Analysis: The Solid-G analysis points out a difference in **2-Y** and **2-Sc** that may be related to their difference in stability. It should be noted that the *G*-parameters are probably best utilized for comparison of complexes within a similar series of ligands. Since the *G*-parameter calculates the total area of the metal coordination sphere shielded by the ligands without distinguishing whether the steric crowding is near or far from the metal center, it is likely best used to compare the steric saturation of ligands with similar shapes. For example, the Cp''_3Ln complexes have all six Me_3Si substituents above and below the plane made by the metal and the centroids, which is different from the three Me_3Si group in Cp'_3Ln which has two above and one below the plane. It is interesting to note that although $Y(OAr')_3$ crystallizes with five different molecules in the unit cell, the *G*-parameters of these five variations are all between 81% and 82%.

The 83% *G*-parameter of [K(crypt)][$Sc(OAr')_3$], **2-Sc**, falls within the range found for a variety of other stable Ln compounds with values roughly between 80% and 90%.[2,15] However the 77% value estimated for "$[Y(OAr')_3]^-$", based on the optimized structure from DFT calculations, is outside the current range of stable species. This means that $[Y(OAr')_3]^-$ is significantly less sterically saturated than the currently-isolable complexes of Y^{II}, [K(crypt)][Cp'_3Y] and [K(crypt)][$Cp''_2Y(C_5H_5)$], which have *G*-parameters of 86% and 90–91%, respectively. It is possible that relatively low coverage of ligands on $[Y(OAr')_3]^-$ makes it too reactive to isolate. In some complexes that would normally have low *G*-parameters, agostic interactions can aid in stabilizing the complex. In the case of $[Y(OAr')_3]^-$, this type of intramolecular interaction would be disfavored by the charge on the complex and the d electron on the metal center. The charge on the complex would also make less favorable the intermolecular interactions of the type found for the polymeric $[(\eta^5\text{-Cp})_2Y(\mu\text{-}\eta^5\text{:}\eta^1\text{-Cp})]_n$.[31]

The transient existence of **2-Dy**, **2-Ho**, and **2-Er** can also be explained by a lack of steric saturation since the size of these metals is similar to that of yttrium. **2-Gd** would be even more sterically unsaturated.

To evaluate the *G*-parameter further, the half-life data on the crystallographically characterized [K(crypt)][Cp'_3Ln] complexes[2] were plotted against their *G*-parameters, Figure 10. The opti-

© 2018 Wiley-VCH Verlag GmbH & Co. KGaA, Weinheim

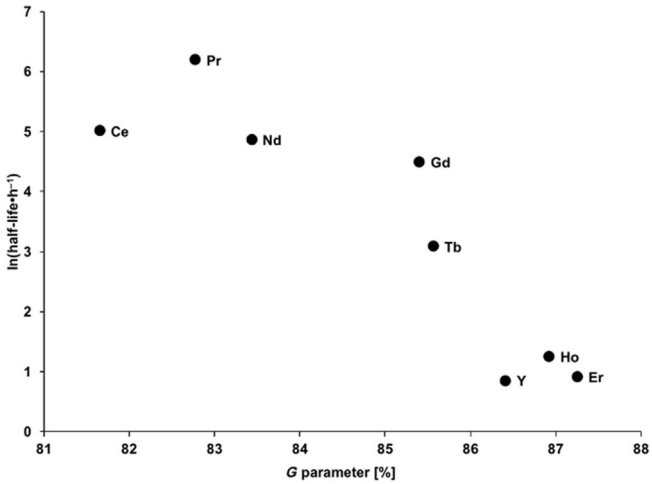


Figure 10. Plot of ln(half-life•h^{-1}) vs. *G*-parameter of the Ln-containing anion for [K(crypt)][Cp′$_3$Ln] at room temperature and 3 mM.

mum thermal stability for this series is found for Ln = Pr, which is neither the most sterically saturated nor unsaturated complex. The range of *G*-parameters may be too narrow to make a definitive correlation, but Figure 10 suggests that within a given series, there could be an optimum *G*-parameter that correlates with stability. More data will be needed to determine if this analysis is more generally applicable. Since OAr′ is a less sterically saturating ligand than Cp′, the only isolable [Ln(OAr′)$_3$]$^-$ complex in the rare earth series may be with the smallest metal, scandium.

Conclusions

Reduction of Ln(OAr′)$_3$ complexes with KC_8 under argon in THF provides EPR evidence for [Ln(OAr′)$_3$]$^-$ complexes of Sc^{II} and Y^{II} and UV/Vis data suggest that similar complexes are generated in solution for Gd, Dy, Ho, and Er. However, only in the case of the smallest metal, Sc, is a crystallographically-characterizable Ln^{II} complex isolated: [K(crypt)][Sc(OAr′)$_3$]. The hyperfine coupling constants suggest that more electron density is on the metal in these [Ln(OAr′)$_3$]$^-$ anions than in analogous complexes of cyclopentadienyl or amide ligands. Analysis of the amount of steric saturation in these aryloxide complexes using the method of Guzei suggests that only with the smallest metal is there sufficient steric saturation to have the necessary thermal stability for crystallization at temperatures above −78 °C. These data provide calibration points to evaluate the effects of steric and electronic factors on the accessibility of Ln^{II} complexes as the ligands are varied.

Experimental Section

All manipulations and syntheses described below were conducted with the rigorous exclusion of air and water using standard Schlenk line and glovebox techniques under an argon atmosphere. Solvents were sparged with UHP argon and dried by passage through columns containing Q-5 and molecular sieves prior to use. Deuterated NMR solvents were dried over NaK alloy or Na/benzophenone, degassed by three freeze-pump-thaw cycles, and vacuum transferred before use. ^{1}H and ^{13}C{^{1}H} NMR spectra were recorded on a Bruker AVANCE600 spectrometer (^{1}H operating at 600 MHz, ^{13}C{^{1}H} at 151 MHz) at 298 K unless otherwise stated and referenced internally to residual protio-solvent resonances. Elemental analyses were conducted on a PerkinElmer 2400 Series II CHNS elemental analyzer. UV/Visible spectra were collected in THF at −78 °C using a Varian Cary 50 Scan UV/Visible spectrophotometer. EPR spectra were collected using X-band frequency (9.3–9.8 GHz) on a Bruker EMX spectrometer equipped with an ER041XG microwave bridge, and the magnetic field was calibrated with DPPH (g = 2.0036). Infrared (IR) transmittance measurements were taken as compressed solids on a Thermo Scientific Nicolet iS5 spectrophotometer with an iD5 ATR attachment. LiOAr′·OEt$_2$ was synthesized by a literature procedure.[35] HOAr′ (Acros) was sublimed before use. 4,7,13,16,21,24-hexaoxa-1,10-diazabicyclo[8.8.8]hexacosane, 2.2.2-cryptand (crypt, VWR) was dried under reduced pressure (10^{-3} torr) before use. KC_8 was synthesized according to literature methods.[36] $LnCl_3$ were prepared according to a literature preparation.[37]

Ln(OAr′)$_3$, 1-Ln: In an adaptation of a literature procedure,[21,38] $LnCl_3$ (1 equiv) and LiOAr′·OEt$_2$ (3 equiv) were heated at reflux overnight in THF under an Ar flow. After cooling to RT, solvent was removed under vacuum to give oily solids. These solids were heated in a boiling water bath and vacuum was applied until solvent evaporation was no longer detected on the vacuum gauge, yielding brittle, dry solids. These solids were loaded into a glass sublimation tube and a plug of glass wool was installed above the solids. The solids were sublimed at 10^{-5} torr and 260 °C overnight. Solids appeared where the tube exited the furnace. The tube was placed deeper into the furnace to re-sublime the solids overnight once more. The resulting highly oxygen- and moisture-sensitive solids were isolated from the sublimation tube in a glove box. The sublimation steps are crucial for purity of the materials.

1-Sc:[23] This complex was prepared as described above with a yield of 1.2 g (66 %) of straw-colored solids. ^{1}H NMR (C_6D_6): δ = 7.08 (s, 6H, C_6H_2), 2.24 (s, 9H, C_6H_2Me), 1.58 ppm (s, 54H, $tBu_2C_6H_2$); ^{13}C{^{1}H} NMR (C_6D_6): δ = 158.2 (*i*-C), 137.2 (*o*-C), 127.5 (*p*-C), 126.3 (*m*-C), 35.2 (CMe_3), 32.3 (CMe_3), 21.5 ppm (C_6H_2Me); IR: $\tilde{\nu}$ = 3069 (w,br), 2956 (m,br), 2919 (m), 2874 (w), 2820 (w), 2734 (w), 1751 (w), 1477 (w), 1456 (m), 1420 (s), 1384 (m), 1354 (m), 1294(w,br), 1261 (m), 1237 (s,br), 1215 (m), 1120 (m), 1041 (w,br), 1023 (w,br), 950 (m), 925 (w,br), 887 (w), 859 (s,br), 808 (m,br), 777 (w,sh), 772 cm^{-1} (m); elemental analysis calcd (5 %) for $C_{45}H_{69}O_3Sc$: C 76.88, H 9.89; found: C 74.21; H 9.48. Results formulate as $C_{45}H_{69}$, but low % composition results across several analyses suggest incomplete combustion of the sample.[1,38–40]

1-Y: This complex was prepared as described above with a yield of 2.3 g (78 %) of white solids. X-ray quality crystals could be grown by slow evaporation of a pentane solution by diffusing the pentane into toluene at −30 °C. ^{1}H NMR (C_6D_6): δ = 7.10 (s, 6H, *m*-C_6H_2), 2.29 (s, 9H, C_6H_2Me), 1.54 ppm (s, 54H, $C_6H_2tBu_2$); ^{13}C{^{1}H} NMR (C_6D_6): δ = 158.41 (*i*-C), 136.8 (*o*-C), 126.2 (*p*-C), 126.0 (*m*-C), 34.7 (CMe_3), 32.0 (CMe_3), 21.6 ppm (C_6H_2Me); IR: $\tilde{\nu}$ = 3065 (w,br), 2956 (m,br), 2912 (m,br), 2873 (w) 2920 (w,sh), 2731 (w), 1756 (w), 1514 (w), 1477 (w,sh), 1457 (m), 1422 (s), 1390 (w,sh), 1358 (m), 1358 (w,sh), 1350 (m), 1325 (w), 1295 (w,br), 1253 (s), 1244 (s), 1213 (m), 1196 (w,sh), 1120 (m), 1204 (w), 949 (w), 922 (w,br), 888 (m), 865 (w,sh), 859 (w), 844 (s), 805 (m), 778 (m), 774 cm^{-1} (m); elemental analysis calcd (%) for $C_{45}H_{69}O_3Y$: C 72.36, H 9.31; found: C 69.50; H 8.96. Multiple attempts gave incomplete combustion as is sometimes observed with rare-earth metal complexes.[1,38–40] However, the observed CH ratio, $C_{45}H_{69}$, matches the calculated.

© 2018 Wiley-VCH Verlag GmbH & Co. KGaA, Weinheim

1-Gd: This complex was prepared as described above with a yield of 87 mg (30%) of white solids. Elemental analysis calcd (%) for $C_{45}H_{69}GdO_3$: C 66.29, H 8.53; found: C 66.15; H 8.58.

1-Dy: This complex was prepared as described above with a yield of 1.5 g, (66%) of beige-to-pink solids. IR: $\tilde{\nu}=3061$ (w), 2955 (m), 2913 (m,br), 1821 (w,br), 2821 (w), 2731 (w), 1456 (s), 1385 (m), 1359 (w,sh), 1350 (w), 1327 (w), 1297 (w), 1244 (s,br), 1312 (m), 1194 (w,sh), 1120 (m), 1023 (w), 949 (w), 924 (w), 888 (w), 865 (w), 860 (w), 842 (s), 804 (m), 778 (w), 774 cm^{-1} (w); elemental analysis calcd (%) for $C_{45}H_{69}DyO_3$: C 65.87, H 8.48; found: C 65.53; H 8.90.

1-Ho: This complex was prepared as described above with a yield of 280 mg (30%) of pink solids. IR: $\tilde{\nu}=3674$ (w,br), 3640 (w,sh), 3626 (w,br), 3071 (w,br), 2953 (s,br), 2912 (s,br), 2871 (m,br), 2731 (w), 1753 (w,br), 1480 (m,sh), 1456 (m), 1420 (s), 1384 (m), 1361 (w), 1349 (w), 1315 (w,sh), 1294 (w,sh), 1246 (s,br), 1214 (m), 1201 (w,sh), 1152 (m,br), 1120 (m), 1039 (w), 1027 (w), 949 (w), 935 (w), 922 (w), 889 (w), 866 (w), 861 (w), 842 (w), 805 (w), 791 (w), 774 (w), 769 cm^{-1} (w); elemental analysis calcd (%) for $C_{45}H_{69}HoO_3$: C 65.68, H 8.45.; found: C 51.36; H 6.78. Incomplete combustion was observed with this compound, but the observed CH ratio, $C_{45}H_{71}$, was close to the calculated.[1,38–40]

1-Er:[20] This complex was prepared as described above with a yield of 1.5 g (65%) of pink-red solids. IR: $\tilde{\nu}=3066$ (w,br), 2960 (m,br), 2916 (m,br), 2867 (w,br), 2814 (w), 2730 (w), 1755 (w,br), 1477 (w,sh), 1457 (m), 1422 (s), 1385 (m), 1369 (w), 1358 (w,sh), 1351 (w,br), 1295 (w,br), 1251 (s,br), 1245 (s,br), 1213 (m), 1196 (m,sh), 1120 (m), 1024 (w), 949 (w), 922 (w,br), 889 (w), 884 (w,sh), 859 (m), 843 (s), 805 (m), 778 (m), 774 cm^{-1} (m).

[K(crypt)][Sc(OAr′)$_3$] 2-Sc: **1-Sc** (100 mg, 0.14 mmol) and crypt (56 mg, 0.15 mmol) were dissolved in a 1:1 THF:Et_2O solution (3 mL) with a glass stir bar and chilled to −30 °C. KC_8 (29 mg, 0.21 mmol, 1.5 equiv) was tapped into the solution with stirring and the mixture immediately turned black. After ca. 1 minute of stirring, the mixture was filtered and the resulting dark maroon solution was layered under −30 °C hexane (10 mL) and stored at −30 °C overnight. The solvent was removed under vacuum to give black solids, which were chilled to −30 °C and triturated with −30 °C pentane (3×1 mL). The pentane was removed under vacuum to give black-purple solids, **2-Sc** (97 mg, 60% yield). X-ray quality crystals could be grown from a THF solution (6 mL) layered under pentane (3 mL) and stored at −30 °C for four days, Figure 2. EPR (Figure 5): $A_{ave}=291$ G, $g_{ave}=2.01$. UV/Vis (Figure 6): λ_{max} (ε): 406 (2100), 522 (2300), 679 nm (790 $M^{-1}cm^{-1}$); IR: $\tilde{\nu}=3739$ (w), 1636 (w), 2952 (m,br), 2891 (m,br), 2817 (w,sh), 2358 (w), 1604 (w), 1477 (m,br), 1456 (m), 1445 (w,br), 1416 (s), 1383 (m), 1374 (w,sh), 1358 (w,sh), 1354 (m), 1292 (w,sh), 1276 (m), 1258 (s), 1248 (s), 1219 (m), 1200 (m,br), 1132 (m), 1103 (s), 1078 (m), 1059 (w), 1025 (w,br), 949 (m), 932 (m), 890 (m), 840 (m,sh), 834 (m), 807 (m), 783 (m), 753 cm^{-1} (m,br); elemental analysis calcd (%) for $C_{63}H_{105}KN_2O_9Sc$: C 67.65, H 9.46, N 2.50; found: C 64.71, H 9.22, N 2.42. Incomplete combustion was observed with this sample but the observed CHN ratio, $C_{63}H_{107}N_2$, matches the calculated.[1,38–40]

2-Ln: A solution of **1-Ln** and crypt (1 equiv) was made in THF (≈1–10 mM, ≈15 mL). A flash reduction column[2,5] was prepared in a glass pipette by tightly packing pieces of a Kimwipe into the bottom of the pipette, with loosely packed Kimwipe above the tightly packed wad, followed by an excess of KC_8 on top of the Kimwipe. The solution, along with the flash reduction column and another glass pipette, were chilled to −30 °C for at least 1 hour. The solution of **1-Ln** and crypt was then added to the flash reduction column using the chilled pipette and mixed with the KC_8 by repeatedly drawing the solution into the chilled pipette and back into the flash column. The solution became a black suspension and then was forced through the Kimwipe to filter it and yield dark-colored **2-Ln**. If the solution was analyzed by UV/Visible spectroscopy, the solution was expressed into a pre-chilled cuvette (1 mm or 1 cm) with a Teflon stopcock, sealed, then placed in a dry ice/isopropanol bath at −78 °C until the spectrum could be acquired (Figure 4 and Figure 8). If the solution was analyzed by EPR spectroscopy, the solution was expressed into a chilled EPR tube in a chilled hexane bath. The EPR tube was then stoppered, quickly removed from the glove box, and frozen in liquid nitrogen.[12]

2-Y: Deep-blue solution. At room temperature, solution fades to colorless in ca. 1 minute. EPR (Figure 3) (THF, 77 K): $A_{ave}=154$ G, $g_{\parallel}=1.99$, $g_{\square}=1.97$; UV/Vis: λ_{max} (ε): 704 nm (6,500 $M^{-1}cm^{-1}$). **2-Gd**: Deep-purple solution. UV/Vis: λ_{max} (ε): 574 (4,500), 434 nm (1,900 sh $M^{-1}cm^{-1}$). **2-Dy**: Deep-purple solution. UV/Vis: λ_{max} (ε): 587 (5,200), 432 nm (3,100 sh). **2-Ho**: Deep-purple solution. UV/Vis: λ_{max} (ε): 579 (2,000), 432 nm (1,200 sh $M^{-1}cm^{-1}$). **2-Er**: Deep-purple solution. UV/Vis: λ_{max} (ε): 583 (6,200), 431 nm (3,600 sh $M^{-1}cm^{-1}$).

Y(OAr)$_3$, 3-Y: Synthesized according to literature procedures.[22] ^1H NMR (C_6D_6): $\delta=7.29$ (d, $J=7.8$ Hz, 6H, *m*-C_6H_3), 6.83 (t, $J=7.8$ Hz, 3H, *p*-C_6H_3), 1.54 ppm (s, 54H, $C_6H_3tBu_2$).

Reduction of 3-Y to form 4-Y: Using the protocol above for producing **2-Y**, a solution of **3-Y** (51 mg, 72 μmol) and crypt (26 mg, 70 μmol) in THF (3 mL) was reduced using a KC_8 flash reduction column, yielding dark-blue **4-Y**. The solution faded to clear and colorless in 1 minute at RT. EPR (Figure S5) (THF, 77 K): $A_{ave}=156$ G, $g_{\parallel}=1.99$, $g_{\square}=1.97$.

Acknowledgements

We thank the U.S. National Science Foundation for support of the synthetic studies (CHE-1565776 to W.J.E) and FONDECYT 1180017/1150629 for support of the computational studies. Furthermore M.J.B.L. acknowledges CONICYT/Doctorado Nacional 2015/21151553 for the Ph.D. fellowship. We also thank Austin J. Ryan for assistance with X-ray crystallography, Professors A. S. Borovik and J. Y. Yang for spectroscopic assistance, and Carter Jones for his CJHUNT (Carter Jones' Highly Useful Numbering Tool) program, which assists in processing crystallography data for use with Solid-G.

Conflict of interest

The authors declare no conflict of interest.

Keywords: aryloxides · low-valent metals · rare-earth metals · reduction · scandium

[1] P. B. Hitchcock, M. F. Lappert, L. Maron, A. V. Protchenko, *Angew. Chem. Int. Ed.* **2008**, *47*, 1488–1491; *Angew. Chem.* **2008**, *120*, 1510–1513.
[2] M. R. MacDonald, J. E. Bates, J. W. Ziller, F. Furche, W. J. Evans, *J. Am. Chem. Soc.* **2013**, *135*, 9857–9868.
[3] M. E. Fieser, M. R. MacDonald, B. T. Krull, J. E. Bates, J. W. Ziller, F. Furche, W. J. Evans, *J. Am. Chem. Soc.* **2015**, *137*, 369–382.
[4] M. R. MacDonald, J. W. Ziller, W. J. Evans, *J. Am. Chem. Soc.* **2011**, *133*, 15914–15917.
[5] M. R. MacDonald, J. E. Bates, M. E. Fieser, J. W. Ziller, F. Furche, W. J. Evans, *J. Am. Chem. Soc.* **2012**, *134*, 8420–8423.
[6] C. T. Palumbo, L. E. Darago, C. J. Windorff, J. W. Ziller, W. J. Evans, *Organometallics* **2018**, *37*, 900–905.

© 2018 Wiley-VCH Verlag GmbH & Co. KGaA, Weinheim

[7] F. Jaroschik, A. Momin, F. Nief, X.-F. Le Goff, G. B. Deacon, P. C. Junk, *Angew. Chem. Int. Ed.* **2009**, *48*, 1117 – 1121; *Angew. Chem.* **2009**, *121*, 1137 – 1141.
[8] F. Jaroschik, F. Nief, X.-F. Le Goff, L. Ricard, *Organometallics* **2007**, *26*, 1123 – 1125.
[9] M. C. Cassani, D. J. Duncalf, M. F. Lappert, *J. Am. Chem. Soc.* **1998**, *120*, 12958 – 12959.
[10] W. J. Evans, D. S. Lee, D. B. Rego, J. M. Perotti, S. A. Kozimor, E. K. Moore, J. W. Ziller, *J. Am. Chem. Soc.* **2004**, *126*, 14574 – 14582.
[11] M. Fang, J. E. Bates, S. E. Lorenz, D. S. Lee, D. B. Rego, J. W. Ziller, F. Furche, W. J. Evans, *Inorg. Chem.* **2011**, *50*, 1459 – 1469.
[12] M. Fang, D. S. Lee, J. W. Ziller, R. J. Doedens, J. E. Bates, F. Furche, W. J. Evans, *J. Am. Chem. Soc.* **2011**, *133*, 3784 – 3787.
[13] Y. K. Gun'ko, P. B. Hitchcock, M. F. Lappert, *J. Organomet. Chem.* **1995**, *499*, 213 – 219.
[14] D. H. Woen, G. P. Chen, J. W. Ziller, T. J. Boyle, F. Furche, W. J. Evans, *Angew. Chem. Int. Ed.* **2017**, *56*, 2050 – 2053; *Angew. Chem.* **2017**, *129*, 2082 – 2085.
[15] A. J. Ryan, L. E. Darago, S. G. Balasubramini, G. P. Chen, J. W. Ziller, F. Furche, J. R. Long, W. J. Evans, *Chem. Eur. J.* **2018**, *24*, 7702 – 7709.
[16] C. T. Palumbo, D. P. Halter, V. K. Voora, G. P. Chen, A. K. Chan, M. E. Fieser, J. W. Ziller, W. Hieringer, F. Furche, K. Meyer, W. J. Evans, *Inorg. Chem.* **2018**, *57*, 2823 – 2833.
[17] M. E. Fieser, C. T. Palumbo, H. S. La Pierre, D. P. Halter, V. K. Voora, J. W. Ziller, F. Furche, K. Meyer, W. J. Evans, *Chem. Sci.* **2017**, *8*, 7424 – 7433.
[18] D. P. Halter, C. T. Palumbo, J. W. Ziller, M. Gembicky, A. L. Rheingold, W. J. Evans, K. Meyer, *J. Am. Chem. Soc.* **2018**, *140*, 2587 – 2594.
[19] I. J. Casely, J. W. Ziller, M. Fang, F. Furche, W. J. Evans, *J. Am. Chem. Soc.* **2011**, *133*, 5244 – 5247.
[20] H. Zhang, R. Nakanishi, K. Katoh, B. K. Breedlove, Y. Kitagawa, M. Yamashita, *Dalton Trans.* **2018**, *47*, 302 – 305.
[21] M. F. Lappert, A. Singh, R. G. Smith, H. A. Stecher, A. Sen, *Synthetic Methods of Organometallic and Inorganic Chemistry*, Georg Thieme Verlag, New York, **1997**.
[22] L. A. M. Steele, T. J. Boyle, R. A. Kemp, C. Moore, *Polyhedron* **2012**, *42*, 258 – 264.
[23] P. B. Hitchcock, M. F. Lappert, A. Singh, *J. Chem. Soc. Chem. Commun.* **1983**, 1499 – 1501.
[24] P. L. Arnold, F. G. N. Cloke, J. F. Nixon, *Chem. Commun.* **1998**, *0*, 797 – 798.
[25] F. G. N. Cloke, K. Khan, R. N. Perutz, *J. Chem. Soc. Chem. Commun.* **1991**, *0*, 1372 – 1373.
[26] R. D. Shannon, *Acta Crystallogr. Sect. A* **1976**, *32*, 751 – 767.
[27] P. Mori-Sánchez, A. J. Cohen, W. Yang, *Phys. Rev. Lett.* **2008**, *100*, 146401 .
[28] T. J. Duignan, J. Autschbach, *J. Chem. Theory Comput.* **2016**, *12*, 3109 – 3121.
[29] L. Maron, O. Eisenstein, *New J. Chem.* **2001**, *25*, 255 – 258.
[30] J. F. Corbey, D. H. Woen, C. T. Palumbo, M. E. Fieser, J. W. Ziller, F. Furche, W. J. Evans, *Organometallics* **2015**, *34*, 3909 – 3921.
[31] M. Adam, U. Behrens, R. D. Fischer, *Acta Crystallogr. Sect. C Cryst. Struct. Commun.* **1991**, *47*, 968 – 971.
[32] R. D. Rogers, J. L. Atwood, A. Emad, D. J. Sikora, M. D. Rausch, *J. Organomet. Chem.* **1981**, *216*, 383 – 392.
[33] M. P. Coles, P. B. Hitchcock, M. F. Lappert, A. V. Protchenko, *Organometallics* **2012**, *31*, 2682 – 2690.
[34] I. A. Guzei, M. Wendt, *Dalton Trans.* **2006**, 3991 – 3999.
[35] B. Çetinkaya, I. Gümrükçü, M. F. Lappert, *J. Am. Chem. Soc.* **1980**, *102*, 2086 – 2088.
[36] D. E. Bergbreiter, J. M. Killough, *J. Am. Chem. Soc.* **1978**, *100*, 2126 – 2134.
[37] M. D. Taylor, *Chem. Rev.* **1962**, *62*, 503 – 511.
[38] N. F. Chilton, C. A. P. Goodwin, D. P. Mills, R. E. P. Winpenny, *Chem. Commun.* **2015**, *51*, 101 – 103.
[39] C. A. P. Goodwin, K. C. Joslin, S. J. Lockyer, A. Formanuik, G. A. Morris, F. Ortu, I. J. Vitorica-Yrezabal, D. P. Mills, *Organometallics* **2015**, *34*, 2314 – 2325.
[40] C. A. P. Goodwin, N. F. Chilton, G. F. Vettese, E. M. Pineda, I. F. Crowe, J. W. Ziller, R. E. P. Winpenny, W. J. Evans, D. P. Mills, *Inorg. Chem.* **2016**, *55*, 10057 – 10067.

Manuscript received: July 26, 2018
Accepted manuscript online: September 10, 2018
Version of record online: November 8, 2018

© 2018 Wiley-VCH Verlag GmbH & Co. KGaA, Weinheim